# Condensation heat transfer coefficient for rectangular multiport microchannels at high ambient temperature

Basim A. R. Al-Bakri[1,2] and Pierre Ricco[1]

[1)] *Department of Mechanical Engineering, The University of Sheffield, Mappin Street, S1 3JD Sheffield, United Kingdom*
[2)] *Department of Engineering Affairs, University of Baghdad, Aljadriya, Baghdad, Iraq*

April 10, 2019

**Abstract**

**Accepted for publication in International Journal of Heat and Mass Transfer**

We experimentally compute the local heat transfer coefficient of blend refrigerant R-410A condensing inside horizontal rectangular multiport aluminium microchannels with hydraulic diameters equal to 0.52 mm and 1.26 mm. The refrigerant flows at near-critical pressure and the cooling air flows at high temperatures proper of hot climates. The experiments are conducted in a bespoke experimental facility and micro-foil sensors are used to measure the local condensation heat flux. The heat transfer coefficient is found to increase with the mass flow rate per unit area and the vapour quality and to decrease with the ambient temperature. Correlations available in the literature do not predict our experimental data satisfactorily because of our extreme operating conditions of high pressure and high cooling air temperature. A novel correlation is therefore obtained to successfully compute the Nusselt number for the condensing annular flow regime in our high pressure and high temperature conditions.

## 1 Introduction

Microchannels are increasingly being utilized in condensers. The rapid development in aluminium extrusion and brazing processes have led to the wide use of this type of condensers. Microchannels produced by these manufacturing technologies have a non-circular multiport structure, with hydraulic diameters of the order of one millimetre. When microchannel condenser with rectangular cross sections are compared with traditional condensers with round cross sections, the former are usually lighter in weight and more compact, and a smaller amount of fluid can be used to dissipate the same heat as in conventional condensers. This helps reduce the energy loss and is beneficial to

the environment. Furthermore, these microchannel condensers are successfully used with blend refrigerants because of their capability to operate under high pressure, which is typical of these refrigerants. Therefore, the technology of these microchannel condensers has paved the way for modern industrial applications, such as electronic cooling for space technology and hot climate air conditioning.

Several studies have focused on measuring and modelling the condensation heat transfer coefficient. Most of these correlations have been developed for flows through large and circular tubes. However, the behaviour of condensing two-phase flow inside non-circular channels, especially with a small hydraulic diameter, is significantly different from those in large circular channels. The condition of near-critical pressure has a significant impact on the condensation heat transfer because the fluid properties in the liquid-vapour dome are considerably different from those at low pressures. Moreover, the coolant type and the cooling conditions targeted to several industrial applications further render the correlations problem specific. It is therefore expected that research works focused on heat transfer in non-circular microchannels with hydraulic diameter smaller than one millimetre are very limited in the literature.

Researchers, such as Yang and Webb (1996a,b, 1997), Webb and Ermis (2001), and Zhang and Webb (2001), have addressed the challenge of measuring and correlating the heat transfer coefficient in horizontal aluminium non-circular multiport channels with hydraulic diameter close to or less than a millimetre for both smooth and internally micro-finned channels. Several correlations have been proposed for the heat transfer coefficient, where the wall-shear stress and the surface tension were included in the formulation.

Investigations on the heat transfer in microchannels with blend refrigerants are even more limited. Kim et al. (2003) conducted an experimental study similar to that of Yang and Webb (1996a,b, 1997) in flat aluminium multichannels with hydraulic diameters of about 1.5 millimetres. Tubes with internal microfins were also tested. The working fluid was R-410A and the results were compared with those of R-22. They found that, at low mass flow rates per unit area, the heat transfer coefficients of R-410A in micro-finned channels were higher than those in smooth channels, and that the heat transfer coefficient decreased with an increase of mass flow rates per unit area. The heat transfer coefficients of R-410A were slightly higher than those of R-22 for smooth channels and the opposite was true for micro-finned channels. Their correlations predicted the experimental data within $\pm 30\%$.

Agarwal et al. (2010) conducted analytical and experimental work for determining the condensation heat transfer coefficients of R-134a in six non-circular horizontal microchannels with hydraulic diameters smaller than a millimetre. The thermal amplification technique developed by Garimella and Bandhauer (2001) was used to measure the heat transfer in small increments of vapour quality across the liquid-vapour dome. It was recommended that the annular flow model be utilized for the squared, parallel-shaped, and rectangular channels, while the mist flow model was used for channels with sharp corners. When comparing these measured data with other correlations, the significant deviation was attributed to the large diameters for which these models were developed.

Cavallini et al. (2005) experimentally measured the heat transfer coefficient and the pressure drop during the condensation of R-134a and R-410A inside multiple parallel 1.4 mm hydraulic diameter channels. The experimental data were compared with different models from the literature and good agreement was obtained with the data of

R-134a, while the same correlations overpredicted the data of R-410A. The discrepancy was attributed to the effect of their smaller diameter compared to those used in other correlations.

The analytical study of Wang and Rose (2005a) showed that the sharpness in the corners of the non-circular channels has a major influence in the condensation process and the liquid film generation. Wang and Rose (2005b) provided a theoretical model for the heat transfer coefficient during condensation in microchannels with squared and triangular cross sections in the hydraulic diameter range of $0.5 - 5$ mm. The mass flow rate per unit area was in the range of $100 - 1300$ kg/m$^2$s for R-134a, R-22, and R-410A. The model was proposed for the annular regime and it was based on the assumption of laminar film condensation flow on the internal walls of the microchannel. The model accounted for the effect of surface tension, interfacial shear stress, and gravity. A significant enhancement of the heat transfer coefficient occurred near the channel entrance due to the surface tension. A general agreement was obtained when the theoretical results were compared with relevant experimental data.

Wu et al. (2009) theoretically developed a three dimensional simulation model for the condensation heat transfer in the annular regime in rectangular channels. The circumference of the inner tube surface was covered with the liquid film and two regions could be distinguished: the thin film region and the meniscus region. The thickness of the condensed film, the wall temperature, and the heat transfer coefficient were computed and the difference between the film and the meniscus condensations in the annular flow regime was addressed.

Garimella et al. (2016) conducted experimental work on near-critical heat transfer with refrigerants R-404A and R-410A in single horizontal round tubes of diameters equal to 3.1, 6.2, and 9.4 mm, and in multiport tubes of diameters equal to 0.76 and 1.52 mm. They used the facility employed earlier by Garimella and Bandhauer (2001) with some modifications to operate at near-critical pressure. They measured the local heat transfer coefficient in small differences of quality for mass flow rate per unit area ranging from 200 to 800 kg/m$^2$s. They found that the existing equations failed to predict the experimental pressure drop and the heat transfer coefficient. Therefore, they used a multi-regime heat transfer model (wavy, annular, and annular/wavy regimes) and found that the annular regime was relevant for microchannel flows. They also proposed an experimental formula based on the Martinelli parameter.

Garimella et al. (2015) experimentally investigated the heat transfer of blend refrigerants R-404A and R-410A in horizontal circular tubes of diameters ranging between 0.76 and 9.4 mm at reduced pressure of $p_r$=1,1.1, and 1.2. The heat transfer coefficient was computed using the overall resistance method. It was found that the spikes of the heat transfer coefficient occurred because of the sharp deviation of the thermodynamic properties at critical temperature. Also, the temperature change had much more effect on the heat transfer coefficient than on the individual change of mass flow rate per unit area. The experimental data were compared with the models for $CO_2$ flow in similar conditions and the results were in poor agreement. They also proposed a new correlation for the gas-coolant heat transfer coefficient at supercritical pressure that predicted the experimental data successfully.

We conclude that there is a dearth of reliable models for the condensation heat transfer coefficient of blend refrigerants flowing in non-circular microchannels with small diame-

ters, operating at near-critical pressure and cooled by air at high ambient temperature. The main objective of this study is therefore, for the first time, to investigate the heat transfer performance of the refrigerant R-410A flowing through horizontal rectangular multiport channels during air-cooled condensation at near-critical pressure and high ambient temperature. A bespoke experimental facility was designed and built for this purpose. The latest technology of the micro-foil heat flux sensor technique was utilized to measure the condensation heat transfer through the microchannel condenser.

Section 2 describes the laboratory apparatus (§2.1), the reduction of the experimental data (§2.2), the heat transfer measurements in single-phase flow conditions (§2.3), and the uncertainty analysis (§2.4). Section 3 presents the results on the dependence of the condensation heat transfer coefficient on the parameters of the system (§3.1), the prediction of our experimental data via existing correlations (§3.2), and our novel correlation for the heat transfer coefficient (§3.3). Section 4 discusses the conclusions of our work.

# 2 Experimental apparatus and procedures

Figure 1 shows the schematic of the experimental apparatus. The sub-cooled liquid refrigerant R-410A, circulated by a variable speed gear pump, flowed into a pre-heater evaporator where it was heated by electrical heaters with a total capacity of 1300 W. The capacity of the heaters was controlled by a variable transformer to achieve the required saturation condition. The refrigerant vapour, generated at the evaporator, entered the test section where it was cooled by an air stream. The condensation process then occurred and the refrigerant phase changed along the channel. The phase of the refrigerant before and after the test section was visualised using a pair of sight glasses. The condensed refrigerant from the test section entered a water-cooled sub-cooler to guarantee that all the refrigerant returned to the initial condition of liquid phase. The sub-cooled liquid refrigerant flowed back to the pump through a Coriolis-effect mass flow meter and a liquid receiver.

The system operating pressure was controlled by an accumulator and a regulating valve, utilizing the nitrogen pressure to stabilise the refrigerant system pressure to the desired value. The amount of circulated refrigerant was controlled by regulating the speed of the pump and by adjusting the flow control valve. A filter dryer was fixed in the section line to remove any possible moisture from the refrigerant during the refrigerant charging process and the channel replacement. The temperature and pressure before and after the evaporator were measured by thermocouples and pressure transducers, respectively. The pressure drop across the test section was measured by a differential pressure transducer.

## 2.1 Test section

The test section, shown in Fig. 2, was composed of two parts: the air duct and the microchannel tubing assembly. The cross-flow air stream flowing over the microchannel was supplied by the air duct and extracted through the duct by a centrifugal fan. The inlet temperature of the cooling air was controlled by a duct heater positioned upstream of the fan and by an integrated temperature control system to guarantee a low level of temperature fluctuations. The tubing assembly was composed of the rectangular aluminium microchannels, mounted horizontally in the air duct and connected to the refrigerant loop

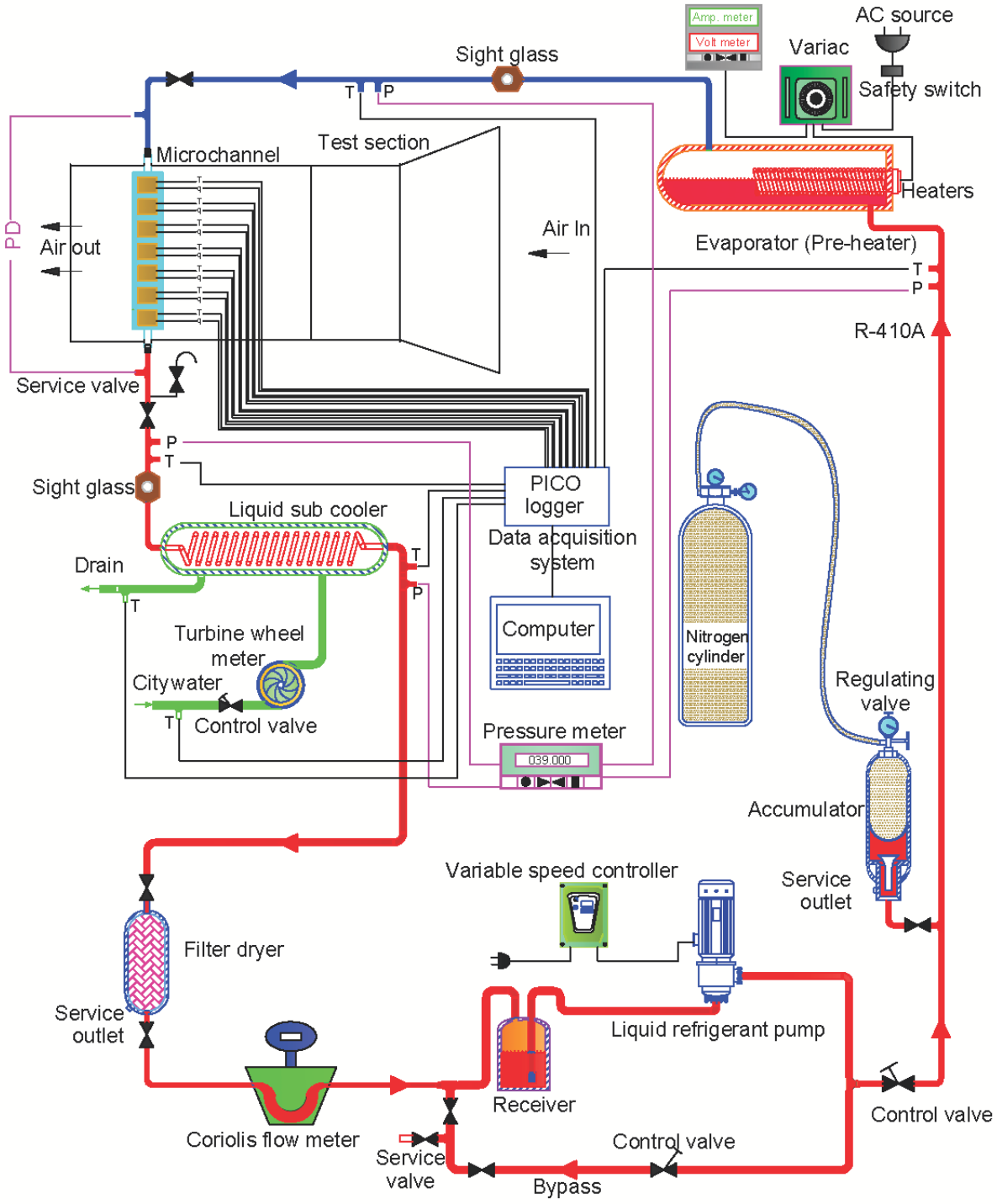


Figure 1: Schematic diagram of the test facility.

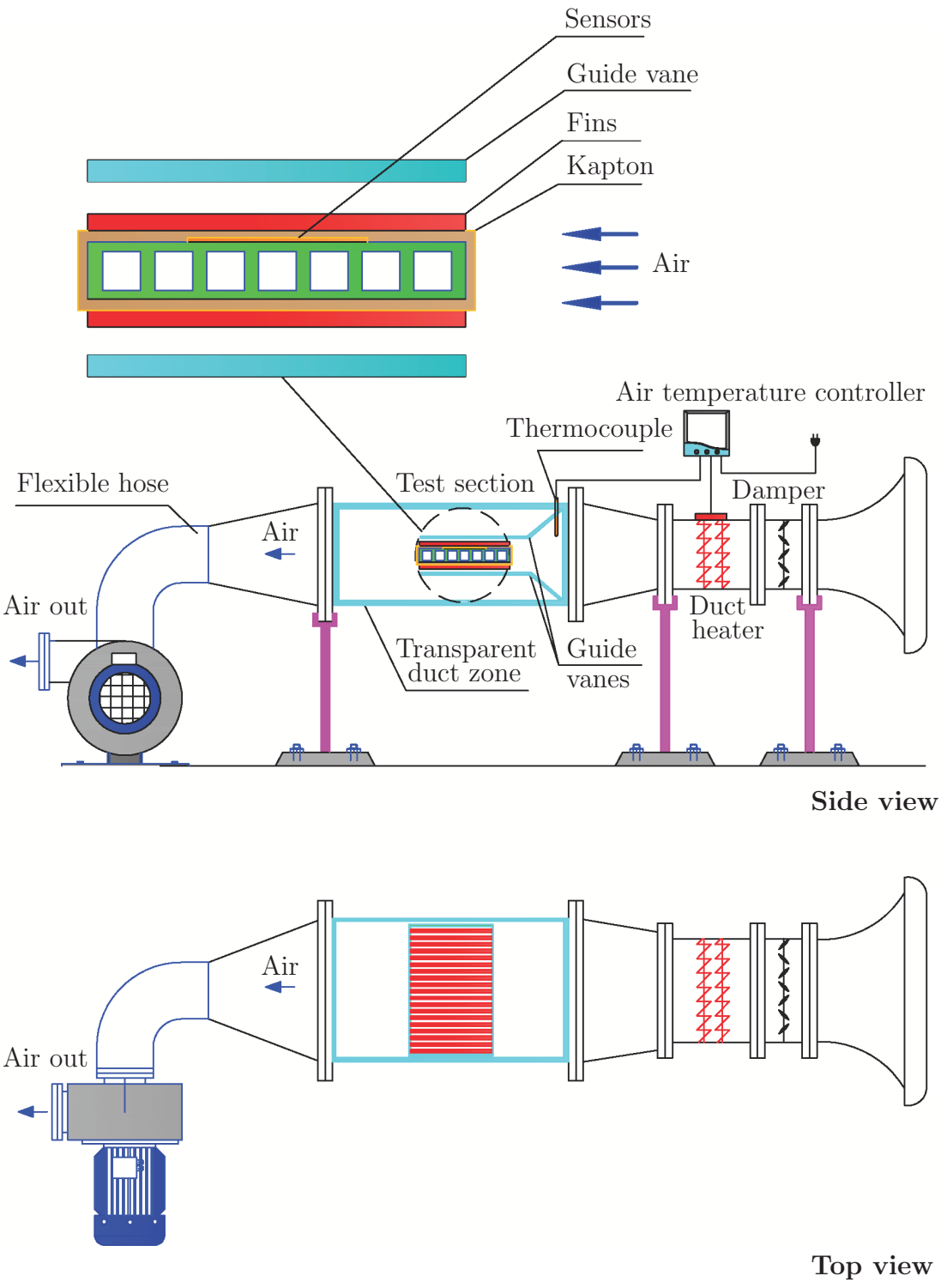


Figure 2: Schematic of the test section.

with a pair of adapters. A sketch of the cross sections of the channels is shown in Fig. 3. Table 1 provides the dimensions of the channels.

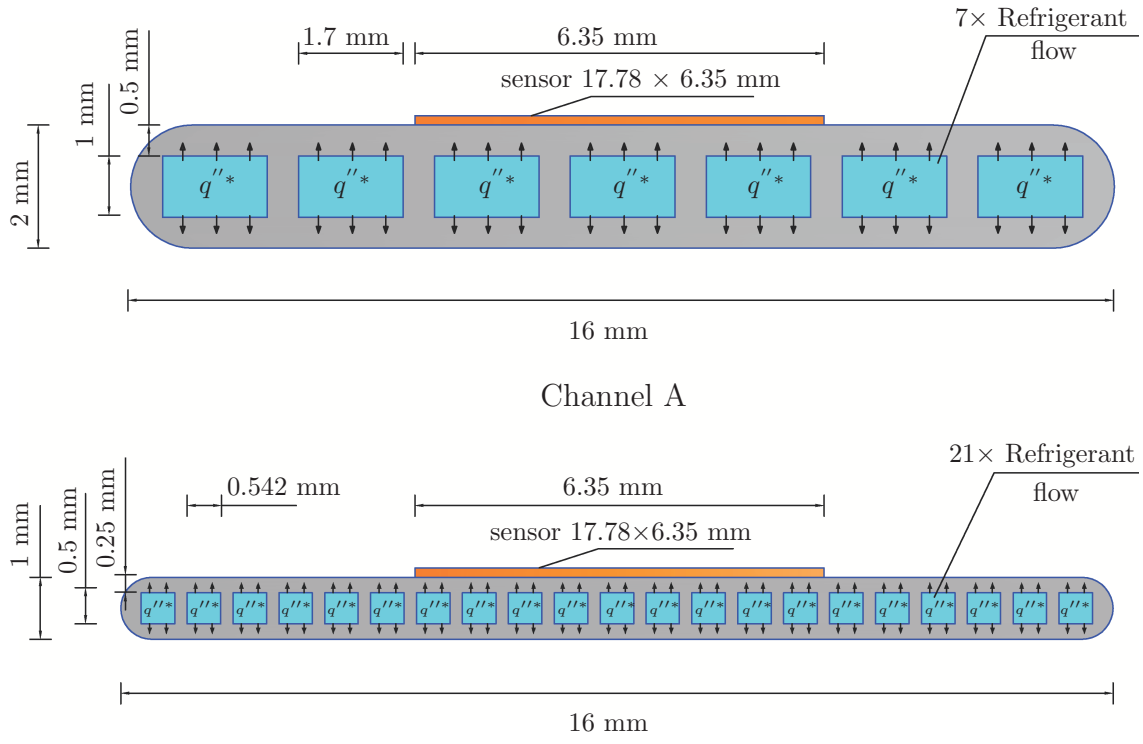


Figure 3: Schematic of the channel cross sections.

| Tube type | Type A | Type B |
|---|---|---|
| Number of channels | 7 | 21 |
| Hydraulic diameter (mm) | 1.26 | 0.52 |
| Channel width (mm) | 16 | 16 |
| Channel length (m) | 0.49 | 0.45 |

Table 1: Dimensions of the microchannels.

Micro-foil heat flux sensors were utilized to measure the local heat flux and the outer surface temperature simultaneously during the condensation process along the channel. A significant feature of the condensation process inside the microchannels is the low mass flow rate per unit area corresponding to a high heat transfer coefficient, which renders these measurements challenging. The specifications of these micro-foil sensors are presented in Table 2. Five micro-foil sensors were mounted to the channel with the 1.26 mm hydraulic diameter, while seven micro-foil sensors were mounted to the channel with the 0.52 mm hydraulic diameter. A data logger employing a pico-software was used to record the sensor readings. The micro-foil sensors were fixed on the outer channel surface at regular intervals along the channel length. These sensors were mounted by wrapping sticky Kapton strips around the channel. To replicate the geometry of the

compact air condenser, straight aluminium fins were placed on the upper and lower outer surface of the channel. They were fixed using a very thin film of thermal paste that introduced a negligible thermal resistance because of its very high thermal conductivity.

| **Model** | **Dimension (mm)** | **Thermo-couples type** | **Nominal sensitivity** $\left(\frac{\boldsymbol{\mu}\mathbf{V}}{\mathbf{W/m^2}}\right)$ | **Maximum heat flux**$<60°\mathbf{C}$ $(\mathbf{W/m^2})$ | **Time constant (s)** | **Maximum operating temp.** $(°\mathbf{C})$ |
|---|---|---|---|---|---|---|
| 27036-1 RdF | $6.35 \times 17.78 \times 0.076$ | T | 0.032 | 568000 | 0.05 | 260 |

Table 2: Specifications of the micro-foil sensors.

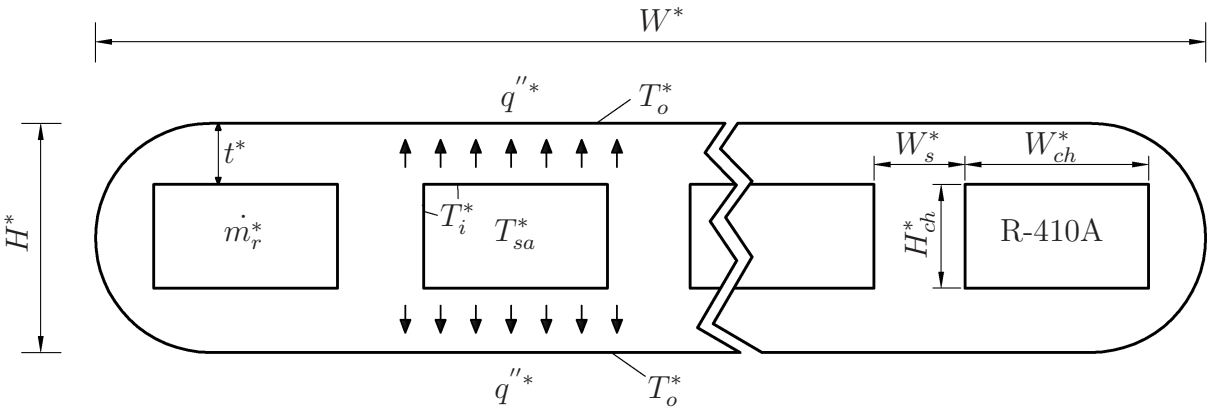


Figure 4: Schematic of channel cross section showing the system parameters used to determine the heat transfer coefficient.

## 2.2 Data reduction

Figure 4 shows the key parameters used to determine the heat transfer coefficient. The local heat flux during the condensation of R-410A was measured directly by the micro-foil heat flux sensors and it was assumed uniform at the outer surface area for each interval along the channel. The main assumptions of the approach were steadiness and one-dimensionality of the heat transfer conduction along the vertical direction, homogeneity and isotropy of the thermal conductivity $k_{ch}^*$ of aluminium, and uniformity of the heat transfer coefficient $h^*$ and of the saturation temperature $T_{sa}^*$ of the refrigerant in cross-sectional planes. Dimensional quantities are henceforth indicated by the superscript $*$.

Thanks to these assumptions and to the symmetry of the channel with respect to the horizontal middle line, each side wall of height $H_{ch}^*$ separating the microchannels could

be treated as two rectangular symmetrical fins. The length of each fin was equal to $H^*_{ch}/2$ and the common fin tip was adiabatic because of the symmetry. The computation of the convection coefficient could thus be carried out by analyzing one half of the channel. From the assumption of one-dimensionality it follows that the temperature of the fin base was equal to the temperature $T_i$ of the top (or bottom) internal surface of each microchannel. As discussed by Qu and Mudawar (2003) and Kim and Mudawar (2010), the heat transfer from both sides of each half microchannel was $\dot{Q}^*_s = \eta_{fin} h^* \Delta L^* H^*_{ch} (T^*_{sa} - T^*_i)$, where $\Delta L^*$ is the length of each measuring interval along the multiport microchannel, $\eta_{fin}$ is the fin efficiency:

$$\eta_{fin} = \frac{\tanh\left(m^* H^*_{ch}/2\right)}{m^* H^*_{ch}/2}, \tag{1}$$

$m^* = \sqrt{2h^*/(k^*_{ch} W^*_s)}$, and $W^*_s$ is the width of the wall between two adjacent microchannels. The heat transfer through the microchannel top (or bottom) internal surface was $\dot{Q}^*_b = h^* \Delta L^* W^*_{ch} (T^*_{sa} - T^*_i)$, where $W^*_{ch}$ is the width of each microchannel. The heat transfer to the exterior from one half of the microchannel was $\dot{Q}^*_{ch} = \dot{Q}^*_s + \dot{Q}^*_b = q^{''*} \Delta L^* (W^*_s + W^*_{ch}) = h^* \Delta L^* (T^*_{sa} - T^*_i)(\eta_{fin} H^*_{ch} + W^*_{ch})$, where $q^{''*}$ is the external heat transfer flux per unit area that was measured directly by the heat-flux sensors and was assumed uniform for each interval along the channel. The fin efficiency $\eta_{fin}$ was computed to be higher than 0.95 and thus assumed to be equal to unity. This proves that the temperature gradient along the side walls could be neglected and the temperature of the side walls could be assumed uniform and equal to $T^*_i$.

The inner surface temperature $T^*_i$ was calculated by the one-dimensional heat conduction balance,

$$T^*_i = T^*_o + \frac{q^{''*}\, t^*}{k^*_{ch}}, \tag{2}$$

where $T^*_o$ is the measured outer surface temperature and $t^*$ is the thickness of the aluminum layer separating the microchannels and the exterior.

The local heat transfer coefficient of condensing R-410A was determined as follows:

$$h^* = \frac{q^{''*}\,(W^*_s + W^*_{ch})}{(T^*_{sa} - T^*_i)\,(H^*_{ch} + W^*_{ch})} = \frac{2W^*}{NP^*} \frac{q^{''*}}{(T^*_{sa} - T^*_i)}, \tag{3}$$

where $W^* = N(W^*_s + W^*_{ch})$ is the multiport microchannel width and $P^* = 2(H^*_{ch} + W^*_{ch})$ is the wetted perimeter of each microchannel. Note that the first expression in (3) coincides with equation (2) in Kim and Mudawar (2010) when $\eta_{fin} = 1$. The factor 2 multiplying $H^*_{ch}$ in their equation (2) is absent in (3) because their microchannel height coincides with half of ours because of the symmetry of our system. The assumption of the temperature of the fin base being equal to $T^*_i$ is further supported by the maximum Biot number of the half wall separating two microchannels being $Bi = h^* W^*_s/(2k^*_{ch}) = 0.01$, thus sufficiently small for the one-dimensionality approximaxtion to be valid.

The local Nusselt number of condensing R-410A was:

$$Nu = \frac{h^*\, D^*_h}{k^*_l}, \tag{4}$$

where $D^*_h = 2W^*_{ch} H^*_{ch}/(W^*_{ch} + H^*_{ch})$ is the hydraulic diameter of the channels and $k^*_l$ is the thermal conductivity of the liquid phase. Another quantity of interest was the

vapour quality, i.e., the mass fraction of vapour in the saturated mixture, denoted by $x$. The vapour quality at the inlet of the test section, $x_{in}$, was determined from the energy balance of the evaporator as:

$$x_{in} = \frac{1}{h^*_{fg}} \left( \mathrm{h}^*_{e,i} + \frac{\dot{Q}^*_e - \dot{Q}^*_{loss}}{\dot{m}^*_r} - \mathrm{h}^*_{e,l} \right), \tag{5}$$

where $\dot{Q}^*_e = I^* V^*$ is the electrical-heater capacity of the evaporator, $I^*$ is the total electrical current of all working heaters, $V^*$ is the voltage, $\dot{Q}^*_{loss}$ is the heat loss to the environment from the evaporator, $\dot{m}^*_r$ is the refrigerant mass flow rate, $h^*_{fg}$ is the latent heat of condensation at the inlet of the test section at its saturation pressure, $\mathrm{h}^*_{e,l}$ is the saturated liquid enthalpy at the evaporator pressure, and $\mathrm{h}^*_{e,i}$ is the liquid enthalpy at the evaporator inlet. The evaporator efficiency was determined when the fluid in the entire rig was in the liquid phase and it could be used when the two-phase flow condition occurred. The evaporator efficiency was defined as:

$$\eta_e = \frac{\dot{Q}^*_e - \dot{Q}^*_{loss}}{\dot{Q}^*_e} = \frac{\dot{m}^*_r (\mathrm{h}^*_{e,o} - \mathrm{h}^*_{e,i})}{\dot{Q}^*_e}, \tag{6}$$

where $\mathrm{h}^*_{e,o}$ is the liquid enthalpy at the evaporator outlet. Equation (5) becomes:

$$x_{in} = \frac{1}{h^*_{fg}} \left( \mathrm{h}^*_{e,i} + \frac{\dot{Q}^*_e \, \eta_e}{\dot{m}^*_r} - \mathrm{h}^*_l \right). \tag{7}$$

The change of vapour quality at each interval along the test section was calculated from the energy balance at different test section intervals as:

$$\Delta x = \frac{2 W^* \, q''^*}{\dot{m}^*_r \, h^*_{fg}} \Delta L^*. \tag{8}$$

We also computed $G^*$, the mass flow rate per unit area, by dividing the mass flow rate by the cross-sectional area of the channels, and the reduced pressure $p_r$ as the ratio of the refrigerant condensation pressure to its critical pressure. The thermodynamic properties of the refrigerant R-410A were calculated using the database of NIST REFPROP version 9.1 (Lemmon et al., 2013) and the tabulated values in the handbook by ASHRAE (2017).

## 2.3 Verification of heat transfer in single-phase flow conditions

Single-phase heat transfer tests were run to verify the thermal performance of the experimental apparatus and instrumentation. The apparatus was operated with the liquid-phase at a system pressure in the range of $30 - 35$ bar, a refrigerant temperature in the range of $35 - 40$°C, and a mass flow rate per unit area in the range of $400 - 800$ kg/m$^2$s. As the heat was extracted by the flowing air, the refrigerant remained in the liquid phase. The energy balance across the test section was applied between the refrigerant side and the average of the sensor measurements of the heat flux. The energy balance index was defined as:

$$e = \frac{(1/N) \sum_{i=1}^{N} q''^*_i}{\dot{m}^*_r \left( \mathrm{h}^*_{l,o} - \mathrm{h}^*_{l,i} \right) / A^*_s}, \tag{9}$$

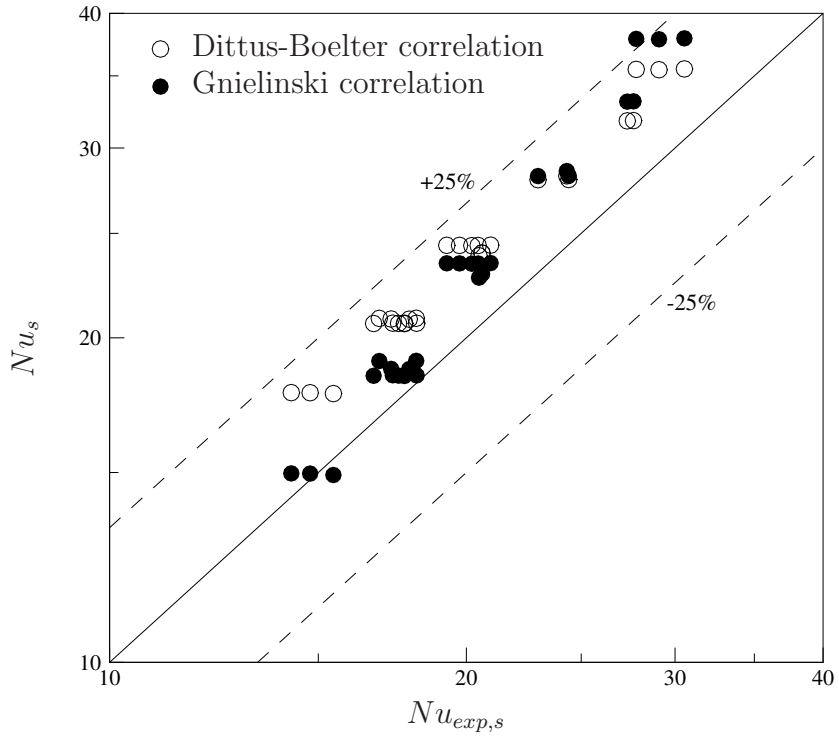


Figure 5: Comparison between our measured single-phase Nusselt numbers $Nu_{exp,s}$ and those computed by the Dittus-Boelter correlation (Dittus and Boelter, 1930) and by the Gnielinski correlation (Gnielinski, 1976).

where $h^*_{l,i}$ and $h^*_{l,o}$ are the liquid enthalpies of the flow before and after the test section, respectively, $q''^*_i$ is the heat flux for each sensor, $N$ is the number of heat flux sensors, and $A^*_s$ is the outer surface area of the channel. The values of $e$ were in the range of $0.87 - 0.96$.

A comparison between our measured single-phase Nusselt numbers and those calculated by the Dittus-Boelter correlation, $Nu_s = 0.023 Re^{0.8} Pr^{0.3}$ (Dittus and Boelter, 1930), and by the Gnielinski correlation, $Nu_s = (f/8)(Re - 1000)Pr/\left[1 + 12.7(f/8)^{0.5}\left(Pr^{2/3} - 1\right)\right]$ (Gnielinski, 1976) (where $Pr$ is Prandtl number and $Re$ is the single-phase Reynolds number based on $D^*_h$ and the mean velocity), was carried out as a further verification of the experimental procedures. The friction coefficient $f$ in the Gnielinski correlation was computed by the first Petukhov correlation, $f = (0.79 \ln Re - 1.64)^{-2}$ (Petukhov, 1970). Figure 5 shows that our data agree better with those computed via the Gnielinski correlation than with those obtained via the Dittus-Boelter correlation, which confirms the discussion on page 319 in Kays and Crawford (1993).

## 2.4 Experimental uncertainty

The experimental uncertainties of the measured parameters were obtained from the calibration of the measuring instruments provided by the manufactures. As an important check of the experimental facility, the measured temperature of the refrigerant at the inlet of the test section was compared with the saturation temperature obtained from the

saturation pressure. The disagreement was below 0.17°C. The uncertainty of the heat transfer coefficient, $U_h^*$, was dominated by the uncertainties of the heat flux, $U_q^*$, and of the temperature difference, $U_{(T_{sa}-T_i)}^*$. It was determined using the method proposed by Moffat (1988) as:

$$U_h^* = \sqrt{\left[\frac{2W^*}{NP^*\left(T_{sa}^* - T_i^*\right)}U_q^*\right]^2 + \left[\frac{2W^*}{NP^*}\frac{q''^*}{\left(T_{sa}^* - T_i^*\right)^2}U_{(T_{sa}-T_i)}^*\right]^2}. \tag{10}$$

The estimated uncertainties of the experimental parameters are presented in Table 3. The dimensions of the cross section of the multiport microchannels were measured using an optical microscope. The channel width was measured by a micrometer with a maximum-error uncertainty of 0.001 mm.

| Parameter | Uncertainty (%) |
|---|---|
| Temperature | ±0.35 |
| $T_{sa}^* - T_i^*$ | ±0.48 |
| Pressure | ±0.025 |
| Pressure difference | ±0.015 |
| Refrigerant mass flow rate | ±0.03 |
| Heat flux | ±1.7 |
| Heat transfer coefficient | ±14 |

Table 3: Uncertainties of the measured quantities.

The mean absolute percentage error between the experimentally measured Nusselt numbers $Nu_{exp}$ and the Nusselt numbers $Nu_{pred}$ predicted by empirical correlations is defined as

$$E(\%) = \frac{100\%}{M}\sum_{i=1}^{M}\frac{|Nu_{i,pred} - Nu_{i,exp}|}{Nu_{i,exp}}. \tag{11}$$

# 3 Results

Tests were conducted on the refrigerant flowing through the microchannels at the two reduced pressures of 0.7 and 0.8 over a range of mass flow rate per unit area of 200 − 800 kg/m$^2$s with a vapour quality ranging between 0.1 and 0.8 along the channel. The condensation process was achieved by utilizing cooling air at the two ambient temperatures of 35°C and 45°C.

## 3.1 Condensation heat transfer coefficient

Figures 6 and 7 illustrate the variation of the local heat transfer coefficient $h^*$ with the vapour quality $x$ for different mass flow rates per unit area for the two reduced pressures, the two ambient air temperatures, and the two channels. The heat transfer coefficient increases with the mass flow rate for all configurations and this change is more significant at high vapour qualities and at high mass flow rates. For small mass flow rates, the heat transfer coefficient changes only slightly as the vapour quality varies considerably.

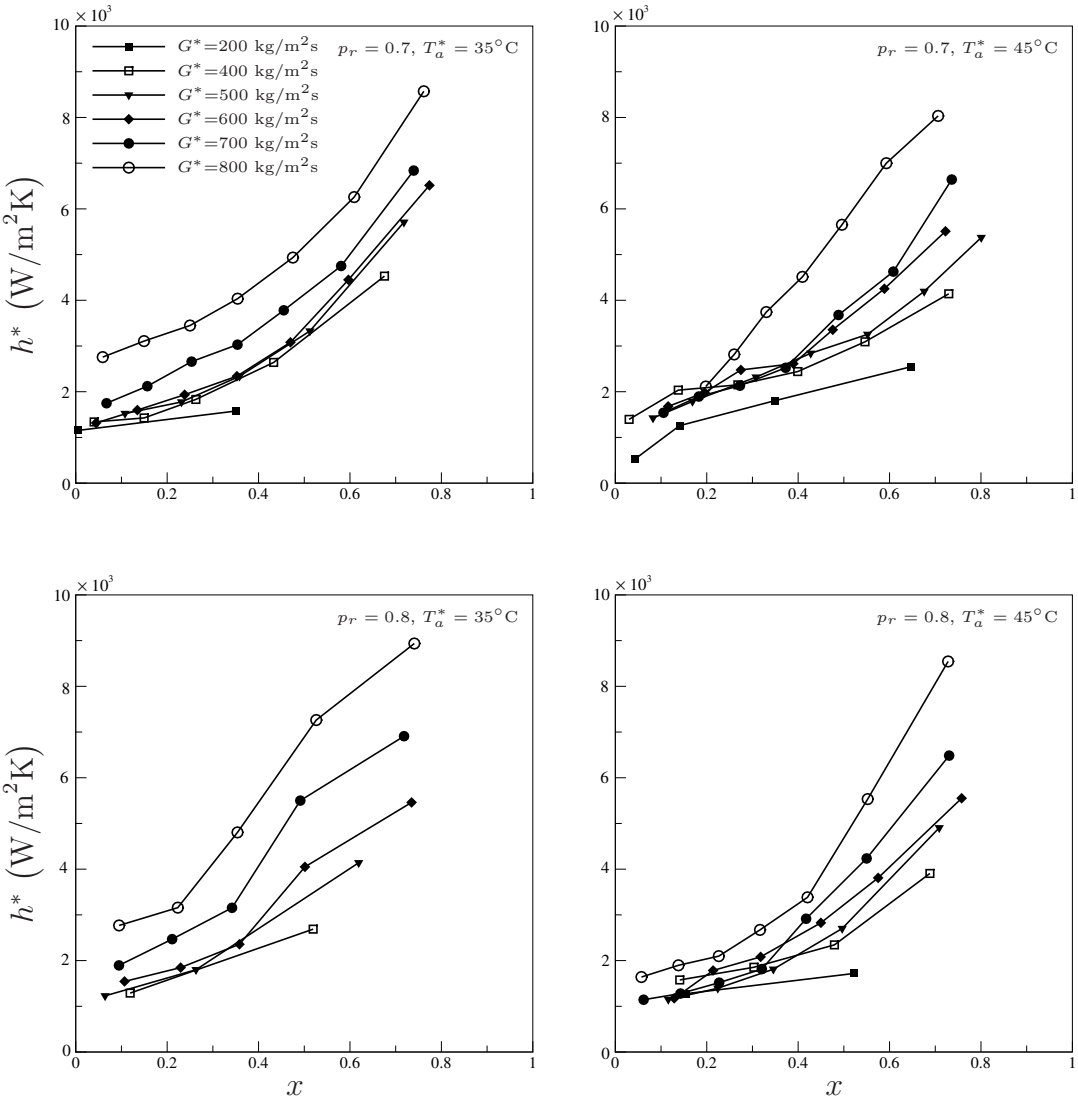


Figure 6: Local condensation heat transfer coefficient $h^*$ of R-410A as a function of the vapour quality $x$ for the two reduced pressures and the two ambient air temperatures for different mass flow rates per unit area. The hydraulic diameter is $D_h^* = 0.52$ mm.

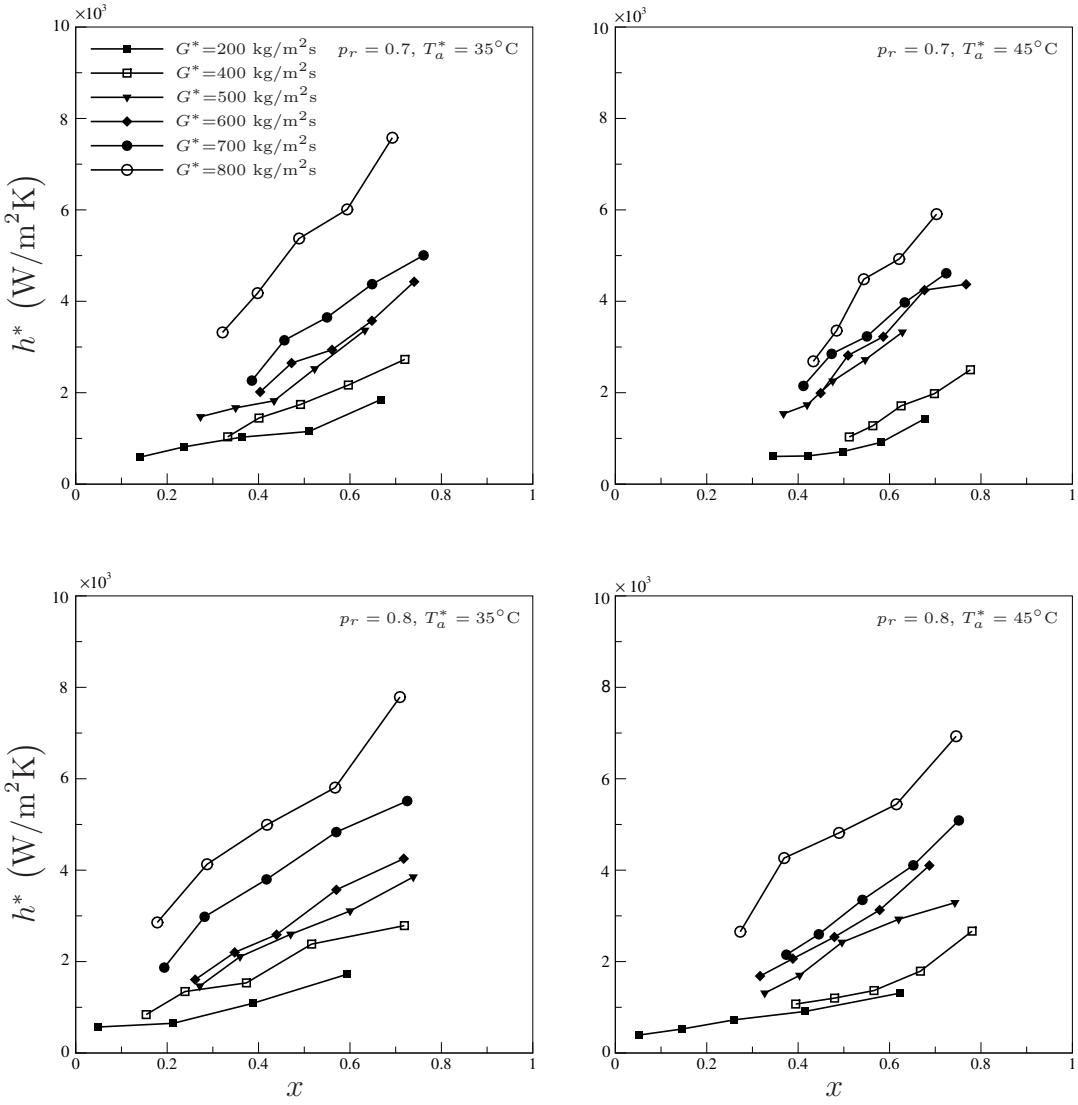


Figure 7: Local condensation heat transfer coefficient $h^*$ of R-410A as a function of the vapour quality $x$ for the two reduced pressures and the two ambient air temperatures for different mass flow rates per unit area. The hydraulic diameter is $D_h^* = 1.26$ mm.

When the condensation process evolves along the channel, the vapour quality substantially decreases from the inlet value. The annular flow regime often occurs due to the channel wall temperature being colder than the fluid temperature, thus creating a liquid film that covers the perimeter of the channel while the vapour flows in the core. The thickness of the liquid film is thus smallest at the inlet where the vapour quality is high. The liquid film thickens as the refrigerant flows along the channel during the condensation process. As a consequence, the heat transfer coefficient is high at high vapour quality because the liquid film that forms on the internal channel surface is thin as the refrigerant is still mostly in the vapour phase. The heat transfer coefficient is large when the vapour quality is large also because of the high specific volume of the vapour phase, which leads to a high vapour core velocity. The heat transfer coefficient in the channel with the small hydraulic diameter, shown in Fig. 6, is higher than in the larger channel, shown in Fig. 7, particularly at high mass flow rates and vapour qualities. As expected, less scatter in the heat transfer coefficient values is found for the larger diameter as the uncertainty of the measurements is lower for that channel. We also observe that at low vapour qualities the heat transfer coefficient of the refrigerant in the small channel varies only slightly although the mass flow rate increases by four times. The slope of the heat transfer coefficient curves becomes sharper for the channel with the small hydraulic diameter, particularly at high mass flow rates. For small vapour qualities, $x < 0.3$, the small-diameter heat transfer coefficient data collapse for most of the mass flow rates. This is likely to be due to the thickness of the liquid film in the annular regime remaining constant. When the reduced pressure increases at constant cooling air temperature, the latent heat of condensation decreases because of the thermodynamic properties of the working fluid. The temperature difference between the inner wall and the saturated fluid increases due to increase of the saturation temperature at approximately constant wall temperature. Therefore, there is no clear evidence of the relation between the heat transfer coefficient and reduced pressure, as shown in Fig. 8.

Figure 9 shows the effect of the ambient air temperature on the local condensation heat transfer coefficient. When the reduced pressure, the mass flow rate per unit area, and the range of the temperature difference between the inner wall and the saturated fluid are constant, the heat transfer coefficient is slightly higher at lower ambient air temperature. Figures 10 and 11 show that the temperature difference between the inner wall temperature and the saturation temperature increases along the channel due to the decrease of the wall temperature. The saturation temperature of the refrigerant is approximately constant along the channel and only very slightly affected by the pressure drop. When the flow is annular, the liquid film thickness increases along the channel due to the condensation process, which leads to a reduction of the wall temperature. The increase of the cooling effect of the wall temperature is linked with the decrease of the condensation heat transfer coefficient. This decrease is due to the development of the liquid layer on the inner perimeter of the multiport channel. The heat transfer coefficient is high when most of the fluid is in the gaseous phase and decreases when the phase changes from gaseous to liquid.

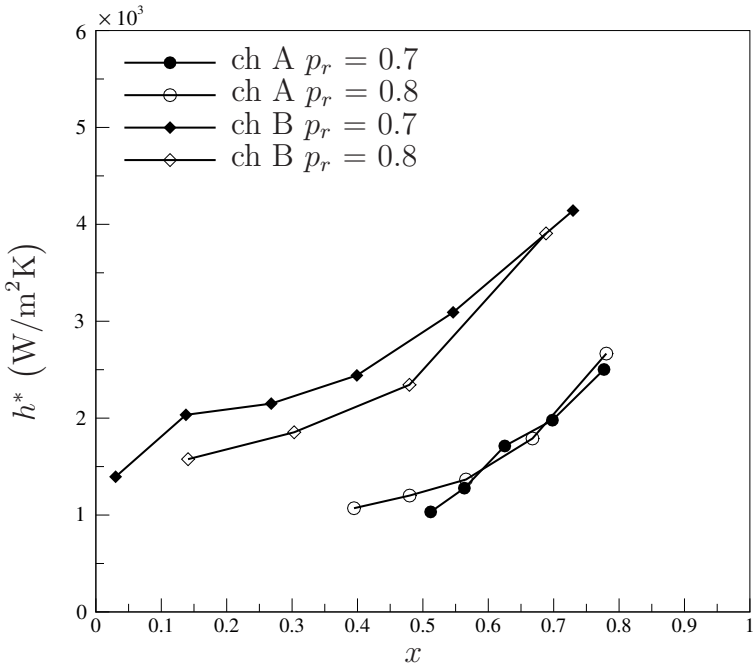


Figure 8: Local condensation heat transfer coefficient $h^*$ as a function of the vapour quality $x$ at two reduced pressures, $p_r = 0.7$ and 0.8, with $T_a^* = 45°\text{C}$ and $G^* = 400$ kg/m$^2$s. The range of $T_{sa}^* - T_i^*$ is $2 - 12°\text{C}$.

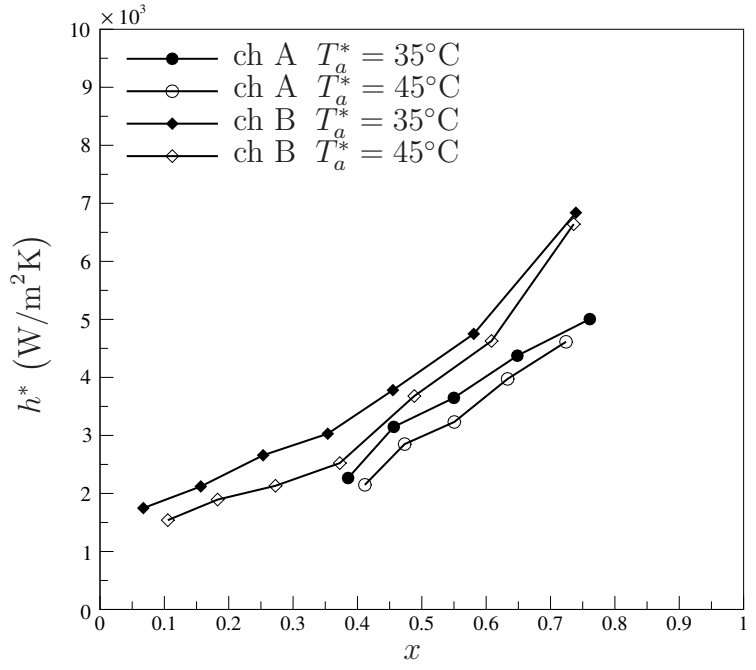


Figure 9: Local condensation heat transfer coefficient $h^*$ as a function of vapour quality $x$ at two ambient air temperatures $T_a^* = 35°\text{C}$ and $T_a^* = 45°\text{C}$ with $p_r = 0.7$ and $G^* = 700$ kg/m$^2$s.

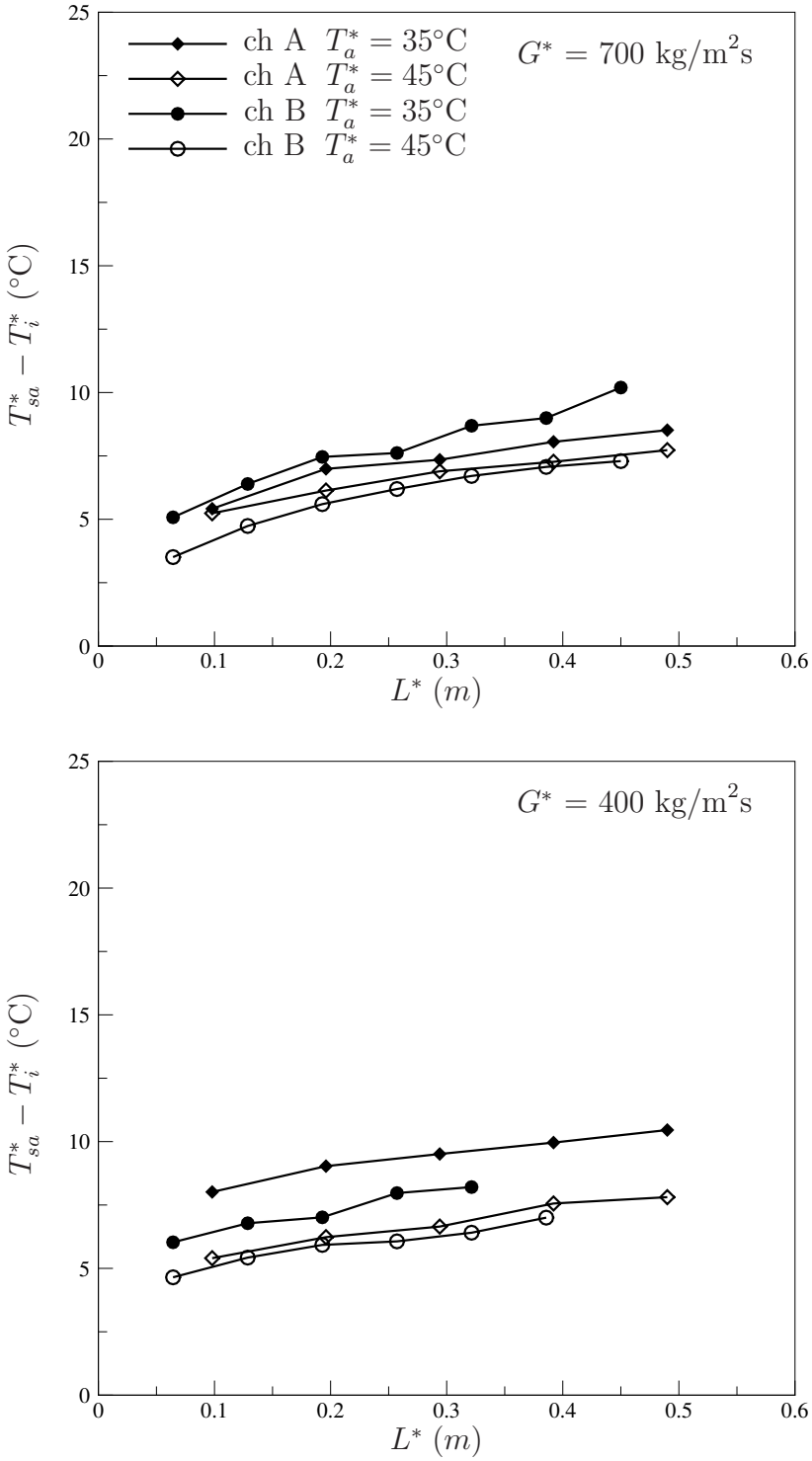


Figure 10: Temperature difference between the inner wall and the saturated liquid as a function of the channel thermal length at two ambient air temperatures $T_a^* = 35°C$ and $T_a^* = 45°C$ with $p_r = 0.7$.

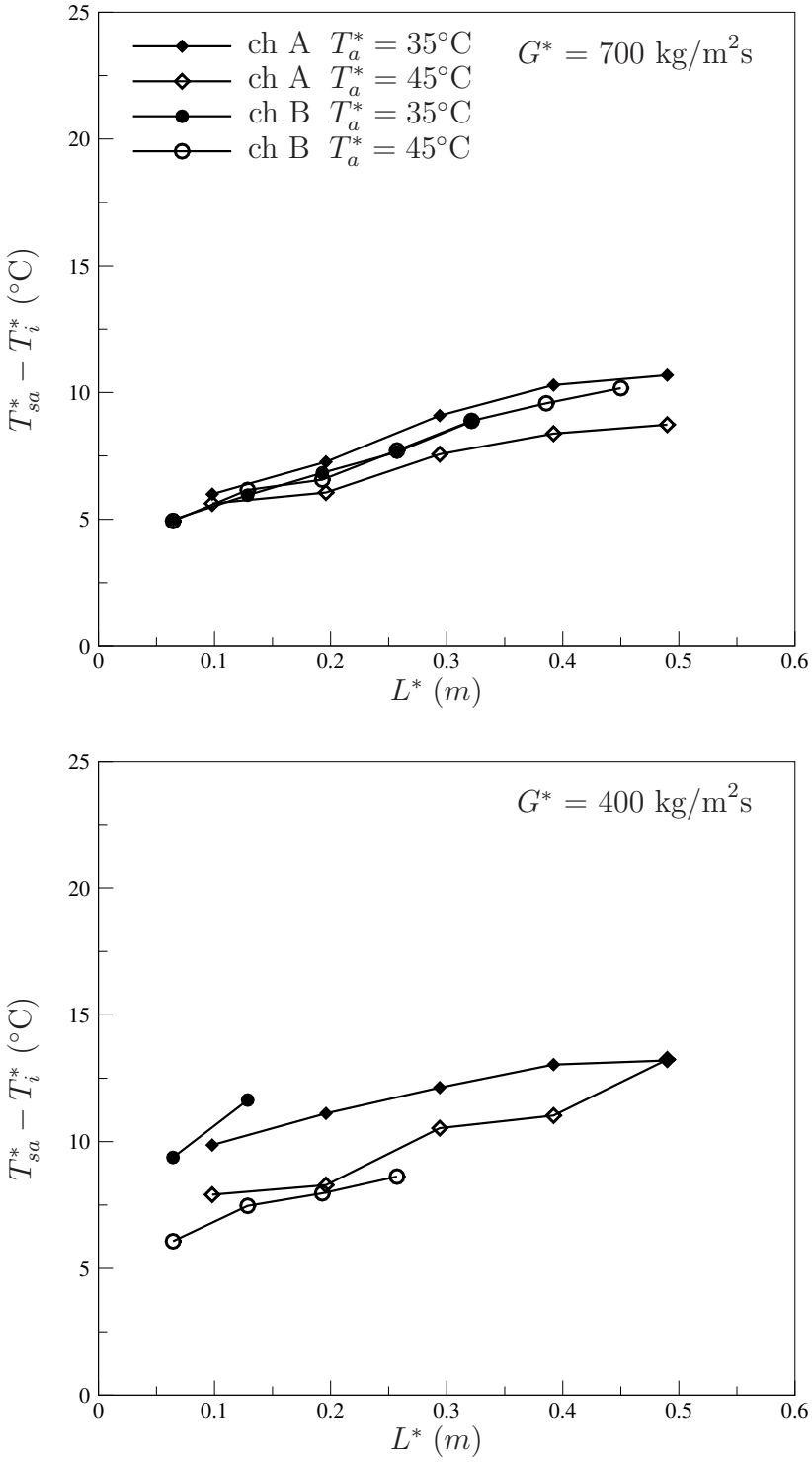


Figure 11: Temperature difference between the inner wall and the saturated liquid as a function of the channel thermal length at two ambient air temperatures $T_a^* = 35°C$ and $T_a^* = 45°C$ with $p_r = 0.8$.

| Authors | Correlations |
|---|---|
| Garimella et al. (2016) | $Nu_{pred} = 0.0133 Re_l^{4/5} Pr_l^{1/3} \left[1 + \left(\frac{x}{1-x}\right)^{0.80} \left(\frac{\rho_l^*}{\rho_g^*}\right)^{0.88}\right]$, where $Re_l = G^*(1-x)D_h^*/\mu_l^*$, $Pr_l = \mu_l^*\ c_{pl}^*/k_l^*$, $G^*$ is the mass flow rate per unit cross-sectional area, $c_{pl}^*$ is the specific heat of the liquid-phase, $\rho_l^*$ and $\rho_g^*$ are the liquid and vapour densities, respectively, and $\mu_l^*$ and $\mu_g^*$ are the liquid and vapour viscosities, respectively. |
| Shah (2016) | $Nu_{pred} = Nu_{lo}\left[1 + 1.128x^{0.817}\left(\frac{\rho_l^*}{\rho_g^*}\right)^{0.3685}\left(\frac{\mu_l^*}{\mu_g^*}\right)^{0.2363}\left(1 - \frac{\mu_g^*}{\mu_l^*}\right)^{2.144} Pr^{-0.1}\right]$<br>$Nu_{lo} = 0.023\left(\frac{G^* D_h^*}{\mu_l^*}\right)^{0.8} Pr_l^{0.4}$ |
| Koyama et al. (2003) | $Nu_{pred} = 0.0152\left(1 + 0.6 Pr_l^{0.8}\right)\frac{\phi_g\, Re_l^{0.77}}{X_{tt}}$<br>$\phi_g^2 = 1 + 21[1 - \exp(-0.319 D_h^*)]X_{tt} + X_{tt}^2$<br>$X_{tt} = \left(\frac{1-x}{x}\right)^{0.9}\left(\frac{\rho_g^*}{\rho_l^*}\right)^{0.5}\left(\frac{\mu_l^*}{\mu_g^*}\right)^{0.1}$ |
| Jige et al. (2016) | $Nu_{pred} = \left(Nu_{An,F}^3 + Nu_{An,S}^3\right)^{1/3}$<br>$Nu_{An,F} = \frac{\phi_g}{1-x}\sqrt{f_g \frac{\rho_l^*}{\rho_g^*}} Re_l^{0.5}\left(0.6 + 0.06 Re_l^{0.4} Pr_l^{0.3}\right)$<br>$Nu_{An,S} = 0.51\left[\frac{\rho_l^* h_{fg}^* \sigma^* D_h^*}{\mu_l^* k_l^* (T_{sa}^* - T_i^*)}\right]^{0.25}$<br>$\phi_g = \sqrt{x^{1.8} + (1-x)^{1.8}\frac{\rho_g^* f_l}{\rho_l^* f_g} + 0.65 x^{0.68}(1-x)^{1.43}\left(\frac{\mu_l^*}{\mu_g^*}\right)^{1.25}\left(\frac{\rho_g^*}{\rho_l^*}\right)^{0.75}}$<br>$f_g = \begin{cases} C_1/(G^* D_h^*/\mu_g^*), & \text{for } G^* D_h^*/\mu_g^* \le 1500 \\ 0.046/(G^* D_h^*/\mu_g^*)^{0.2}, & \text{for } G^* D_h^*/\mu_g^* > 1500 \end{cases}$<br>$f_l = \begin{cases} C_1/(G^* D_h^*/\mu_l^*), & \text{for } G^* D_h^*/\mu_l^* \le 1500 \\ 0.046/(G^* D_h^*/\mu_l^*)^{0.2}, & \text{for } G^* D_h^*/\mu_l^* > 1500 \end{cases}$<br>$C_1 = 24\left(1 - 1.355\mathcal{A} + 1.947\mathcal{A}^2 - 1.701\mathcal{A}^3 + 0.956 A^4 - 0.254\mathcal{A}^5\right)$, where $\mathcal{A}$ is the aspect ratio of the microchannels. |

Table 4: Correlations of Nusselt numbers.

## 3.2 Comparison with existing heat transfer correlations

Various approaches for predicting the heat transfer coefficients during condensation have been presented in the literature. Three main categories can be identified: the two-phase multiplier approach, the boundary layer approach, and the shear force approach. The present experimental data were compared with the predictions obtained by different correlations, i.e., those by Garimella et al. (2016) and Shah (2016) based on the multiplier approach, the one by Koyama et al. (2003) based on the boundary layer approach, and the one by Jige et al. (2016) based on the shear force approach. Most of the correlations overpredict our heat transfer coefficients because either the channel diameters used for those correlations were larger and circular or they do not account for flow phenomena that are specific to microchannels in our conditions of near-critical pressure and high coolant air temperature. Table 4 summarizes the correlations used to predict our experimental data.

Garimella et al. (2016) utilized a correlation similar to the one proposed by Cavallini and Zecchin (1974), but the regression analysis was carried out using their own experimental data. Garimella et al. (2016)'s correlation predicts our experimental data with $E = 50\%$ for channels A and B, as shown in Fig. 12. Although Garimella et al. (2016) also used R-410A, with nearly the same reduced pressure, their predicted values correlate poorly with our measured data. This is arguably because their range of diameters was much larger than ours, their tube had a round cross section while our channels were rectangular, and they used water at low temperature as coolant, while our cooling fluid was air at high temperature. In addition, their correlation does not account for the effect of reduced pressure. The comparison with Shah (2016)'s correlation, shown in Fig. 13, is not satisfactorily as it highly overpredicts our Nusselt number data. Shah (2016) used the correlations of Shah (1979) and Cavallini et al. (2006), but they employed the methodology by Shah (2013) to calculate the heat transfer coefficient.

Figure 14 shows the comparison between our local experimental Nusselt number $Nu_{exp}$ and that predicted by Koyama et al. (2003). Their correlation gives the best overall agreement, especially at high mass flow rates and for the flow through the large channel. For low mass flow rates the agreement is not as satisfactory since their correlation includes the effect of the wavy annular flow that is unlikely to occur in our case, especially in the channel with the small hydraulic diameter. Part of the data is predicted within $E = 30\%$. Figure 15 shows the comparison between our experimental data and the prediction by Jige et al. (2016)'s correlation. Their correlation leads to similar agreement to that given by Koyama et al. (2003)'s correlation, i.e., within $E = 30\%$ for most of our Nusselt number data. Koyama et al. (2003) and Jige et al. (2016) used the methodology by Haraguchi et al. (1994), which combines the effects of the annular regime and gravity.

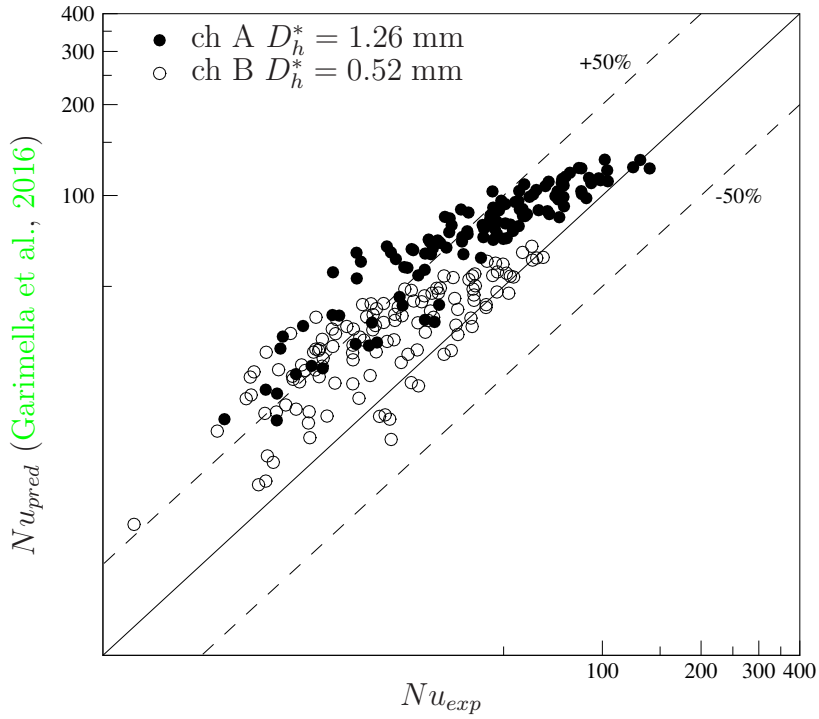


Figure 12: Comparison between the experimentally measured Nusselt number $Nu_{exp}$ and the Nusselt number $Nu_{pred}$ predicted by Garimella et al. (2016)'s correlation.

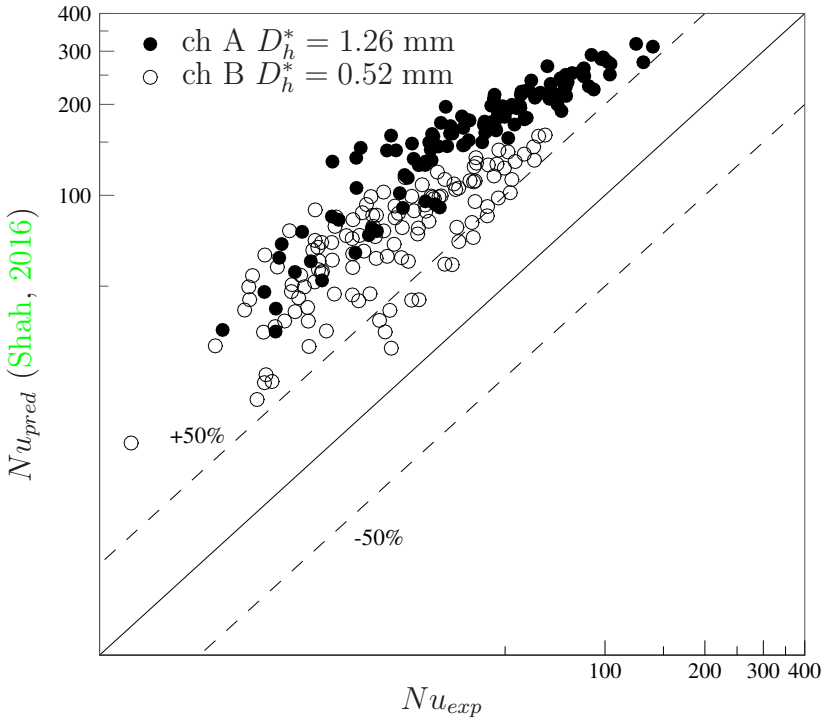


Figure 13: Comparison between the experimentally measured Nusselt number $Nu_{exp}$ and the Nusselt number $Nu_{pred}$ predicted by Shah (2016)'s correlation.

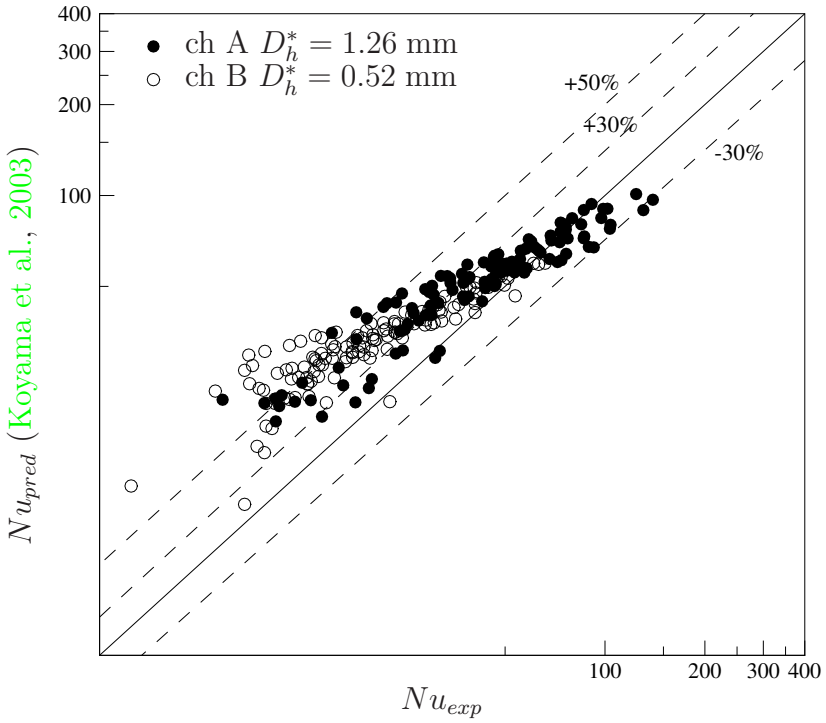


Figure 14: Comparison between the experimentally measured Nusselt number $Nu_{exp}$ and the Nusselt number $Nu_{pred}$ predicted by Koyama et al. (2003)'s correlation.

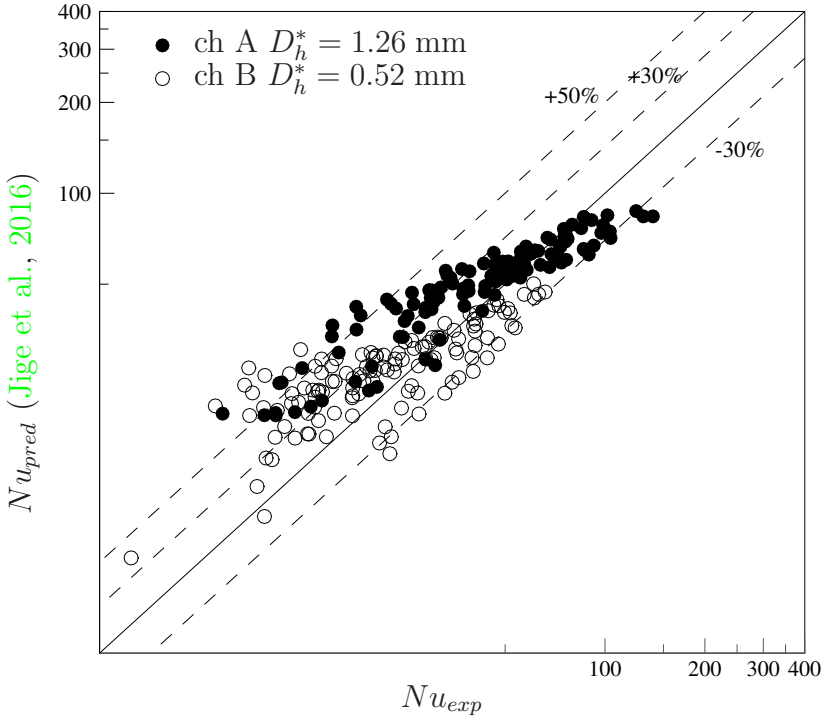


Figure 15: Comparison between the experimentally measured Nusselt number $Nu_{exp}$ and the Nusselt number $Nu_{pred}$ predicted by Jige et al. (2016)'s correlation.

### 3.3 Novel correlation of the condensation heat transfer coefficient

Most of our data are within the range of dimensionless superficial velocity $J_G = G^* x \left[D_h^* g^* \rho_g^* (\rho_l^* - \rho_g^*)\right]^{-1/2} \geq 2.5$, where $g^*$ is the gravitational acceleration, and therefore, as shown by Cavallini et al. (2002), the annular regime dominated in both channels. For small hydraulic diameters the annular flow is likely to occur because of the significant shear forces. This is because the surface tension dominates over gravity when the diameter is small, as discussed by Nema et al. (2014), who identified the transition criterion to distinguish between the effects of surface tension and gravity forces in microchannel flows. Furthermore, the non-circular cross section helps perpetuate the annular flow regime even at low mass flow rates and for a wide range of vapour qualities. Indeed, the non-circular geometry causes a pressure reduction at the corners due to the curvature of the liquid-vapour-interface, which tends to drive more liquid to the corners and maintain the annular flow regime. This is known as the Gregorig effect (Gregorig, 1962). Also, when the condensation process occurs near the critical pressure, the properties of the liquid and vapour become similar which means that the annular flow occurs for a wide range of vapour quality and mass flow rates.

Only the data that satisfied the annular flow inequality proposed by Cavallini et al. (2002) were considered to obtain an empirical correlation of the Nusselt number as a function of independent dimensionless parameters. The Nusselt number is written as:

$$Nu_{pred} = f(Re_l, Pr_l, p_r, X_{tt}) = A\ Re_l^n\ Pr_l^{n_1}\ p_r^{n_2}\ X_{tt}^{n_3}, \tag{12}$$

where $A$, $n, n_1, n_2$, and $n_3$ are constants found through a non-linear regression analysis. The empirical correlation is:

$$Nu_{pred} = 0.018\ Re_l^{0.94}\ Pr_l^{-0.22} p_r^{1.4} X_{tt}^{-1.04}. \tag{13}$$

Figure 16 shows the comparison between our experimental data and the prediction obtained with our correlation (13). The present correlation successfully predicts the experimental data with $E = 25\%$, more accurately than any other correlation available in the literature.

## 4 Conclusions

We have experimentally studied the local heat transfer coefficient of the refrigerant R-410A during condensation inside horizontal multiport aluminium microchannels of rectangular cross section with hydraulic diameters $D_h^* = 0.52$ mm and $D_h^* = 1.26$ mm at two reduced pressures, $p_r = 0.7$ and $p_r = 0.8$. The condensation process was accomplished using air as the coolant at two temperatures, $T_a^* = 35°$C and $T_a^* = 45°$C. The experimental technique adopted in this study allowed the direct measurement of the two key parameters needed for calculating the local heat transfer coefficient, i.e., the local heat flux during condensation along the channel and the temperature difference.

The condensation heat transfer coefficient increases with an increase of refrigerant mass flow rate per unit area and vapour quality and it is larger for the flow in the smaller hydraulic diameter. At high mass flow rates per unit area and vapour qualities

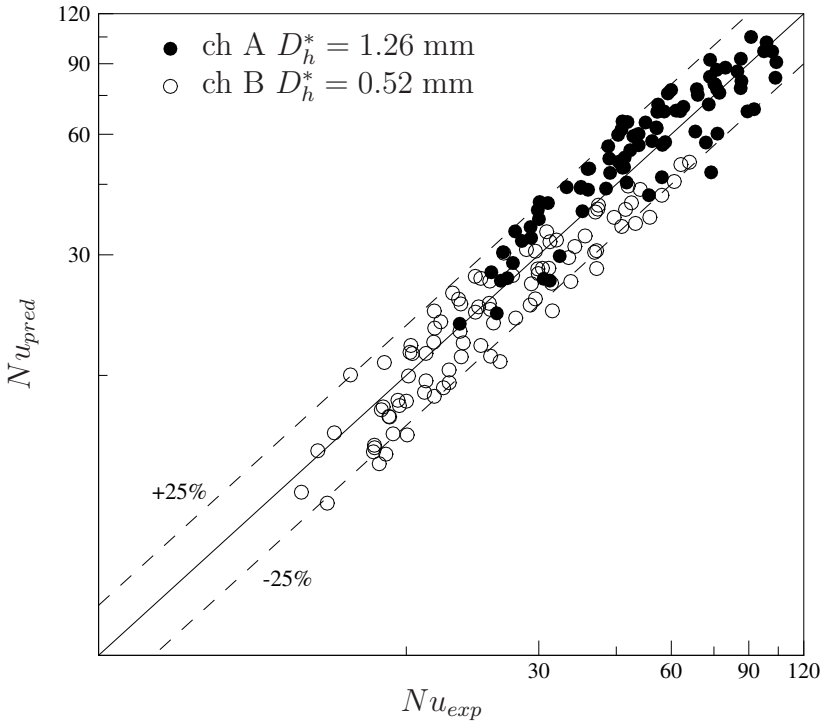


Figure 16: Comparison between the experimentally measured Nusselt number $Nu_{exp}$ and the Nusselt number $Nu_{pred}$ predicted by correlation (13).

for a low reduced pressure, the heat transfer coefficient is slightly larger for a lower ambient air temperature. The prediction of the experimental data through correlations available in the literature was found to be unsatisfactory mainly because of our extreme conditions of operation, i.e., high ambient temperature and near-critical pressure. Only the predictions by the correlations of Koyama et al. (2003) and Jige et al. (2016) offered a modest agreement with our experimental data, but this was limited to high values of the vapour quality for the flow in the larger channel. A new empirical correlation for the local heat transfer coefficient for the annular flow regime was obtained to predict our experimental data successfully.

The next research step is to extend the present analysis to investigate the heat transfer for the refrigerant R-410A at critical conditions. In the facility used in our study, the critical conditions would be achieved at a pressure of approximately 50 bar. The comparison between the near-critical and critical heat transfer coefficient would be extremely beneficial for a comprehensive understanding of condensation heat transfer in microchannels. Further interesting aspects to be explored are the effect of free-stream turbulence of the oncoming cooling stream on the microchannel heat transfer and the flow visualization at high operating pressure during the condensation process. The latter represents a challenge because of the difficulty in using a transparent material suitable for the flow visualization that is also able to sustain near-critical or even critical pressure.

# Acknowledgement

The financial support of the Iraqi Ministry of Higher Education and Scientific Research is highly acknowledged.


# Nomenclature

| | |
|---|---|
| $A_s^*$ | outer surface area of the channel, $mm^2$ |
| $c_p^*$ | specific heat, J/kg K |
| $D_h^*$ | microchannel hydraulic diameter, mm |
| $e$ | energy balance index |
| $G^*$ | mass flow per unit cross-sectional area, $kg/m^2s$ |
| $g^*$ | gravitational acceleration, $m/s^2$ |
| $h^*$ | local heat transfer coefficient, $W/m^2\,K$ |
| $H_{ch}^*$ | internal height of each microchannel, mm |
| $h_l^*$ | saturated liquid enthalpy at the evaporator pressure, J/kg |
| $h_e^*$ | enthalpy, J/kg |
| $h_{fg}^*$ | latent heat, J/kg |
| $J_G$ | scaled superficial velocity |
| $k^*$ | thermal conductivity, W/m K |
| $L^*$ | length of the multiport microchannel, mm |
| $\dot{m}^*$ | mass flow rate, kg/s |
| $N$ | number of microchannels |
| $Nu$ | Nusselt number |
| $P^*$ | wetted perimeter of each microchannel |
| $Pr$ | Prandtl number |
| $p^*$ | pressure, Pa |
| $p_r$ | reduced pressure, $p^*/p_{critical}^*$ |
| $\dot{Q}^*$ | heat transfer, W |

458 $q''^{*}$ local external heat flux measured by the sensors, W/m$^2$

459 $Re$ Reynolds number based on $D_h^*$ and bulk velocity

460 $T^*$ temperature, °C

461 $t^*$ channel thickness, mm

462 $W^*$ width of multiport channel, mm

463 $W_{ch}^*$ internal width of each microchannel, mm

464 $W_s^*$ width of wall separating adjacent microchannels, mm

465 $X$ Lockhart-Martinelli parameter

466 $x$ vapour quality

# 467 Greek symbols

468 $\Delta L^*$ thermal length of each interval along the channel, mm

469 $\Delta x$ vapour quality difference

470 $\mu^*$ dynamic viscosity, kg/m s

471 $\rho^*$ density, kg/m$^3$

472 $\eta$ fin efficiency

473 $\phi$ two-phase pressure drop multiplier

# 474 Subscripts

475 $a$ air

476 $ch$ channel

477 $e$ evaporator

478 $exp$ experimental

479 $g$ gas phase

480 $l$ liquid phase

481 $lo$ liquid only

482 $loss$ heat loss

483 $w$ wall

484 $i$ in/inner

485 $o$ out/outer

*pred* predicted

*r* refrigerant

*sa* saturation

*tt* turbulent liquid-turbulent vapour

# References


Agarwal, A., Bandhauer, T. M. and Garimella, S. (2010). Measurement and modelling of condensation heat transfer coefficients in non-circular microchannels, *Int. J. Refrig.*, **33 (6)**: 1169–1179.

ASHRAE (2017). *2017 ASHRAE Handbook-Fundamentals*.

Cavallini, A., Censi, G., Del Col, D., Doretti, L., Longo, G. A. and Rossetto, L. (2002). Condensation of halogenated refrigerants inside smooth tubes, *HVAC and R Research*, **8 (4)**: 429–451.

Cavallini, A., Del Col, D., Doretti, L., Matkovic, M., Rossetto, L. and Zilio, C. (2005). Condensation heat transfer and pressure gradient inside multiport minichannels, *Heat Tran. Eng.*, **26 (3)**: 45–55.

Cavallini, A., Del Col, D., Doretti, L., Matkovic, M., Rossetto, L., Zilio, C. and Censi, G. (2006). Condensation in horizontal smooth tubes: a new heat transfer model for exchanger design, *Heat Tran. Eng.*, **27 (8)**: 31–38.

Cavallini, A. and Zecchin, R. (1974). A dimensionless correlation for heat transfer in forced convection condensation, *Proc. Sixth Int. Heat Tran. Conf.*, **3**: 309–313.

Dittus, F. and Boelter, L. (1930). Publications on engineering, vol. 2, *University of California at Berkeley, Berkeley, CA*, pp. 443–461.

Garimella, S., Andresen, U., Mitra, B., Jiang, Y. and Fronk, B. (2016). Heat transfer during near-critical-pressure condensation of refrigerant blends, *J. Heat Tran.*, **138 (5)**: 051503.

Garimella, S. and Bandhauer, T. M. (2001). Measurement of condensation heat transfer coefficients in microchannel tubes, *American Soc. Mech. Eng., Heat Transfer Division, (Publication) HTD*, **369**: 243–249.

Garimella, S., Mitra, B., Andresen, U. C., Jiang, Y. and Fronk, B. M. (2015). Heat transfer and pressure drop during supercritical cooling of HFC refrigerant blends, *Int. J. Heat Mass Tran.*, **91**: 477 – 493.

Gnielinski, V. (1976). New equations for heat and mass transfer in turbulent pipe and channel flow, *Int. Chem. Eng.*, **16 (2)**: 359–368.

519 Gregorig, R. (1962). Verfahrenstechnisch günstigere führung der mittel der
520 wärmeübertragung beim verdampfen und kondensieren, *Int. J. Heat Mass Tran.*, **5 (3-**
521 **4)**: 175–188.

522 Haraguchi, H., Koyama, S. and Fujii, T. (1994). Condensation of refrigerants HCFC22,
523 HFC134a and HCFC123 in a horizontal smooth tube (1st report, proposal of empirical
524 expressions for the local frictional pressure drop), *Trans JSME (B)*, **60 (574)**: 239–44,
525 in Japanese.

526 Jige, D., Inoue, N. and Koyama, S. (2016). Condensation of refrigerants in a multiport
527 tube with rectangular minichannels, *Int. J. Refrig.*, **67**: 202 – 213.

528 Kays, W. and Crawford, M. (1993). *Convective Heat and Mass Transfer*, McGraw-Hill,
529 third edn.

530 Kim, N.-H., Cho, J.-P., Kim, J.-O. and Youn, B. (2003). Condensation heat transfer of
531 R-22 and R-410A in flat aluminum multi-channel tubes with or without micro-fins, *Int.*
532 *J. Refrig.*, **26 (7)**: 830–839.

533 Kim, S.-M. and Mudawar, I. (2010). Analytical heat diffusion models for different micro-
534 channel heat sink cross-sectional geometries, *Int. J. Heat Mass Trans.*, **53 (19-20)**:
535 4002–4016.

536 Koyama, S., Kuwahara, K., Nakashita, K. and Yamamoto, K. (2003). An experimental
537 study on condensation of refrigerant R-134a in a multi-port extruded tube, *Int. J.*
538 *Refrig.*, **26 (4)**: 425–432.

539 Lemmon, E., Huber, M. and McLinden, M. (2013). *NIST Standard Reference Database 23:*
540 *NIST Reference Fluid Thermodynamic and Transport Properties -REFPROP, Version*
541 *9.1*, NIST, Gaithersburg, Maryland, US.

542 Moffat, R. J. (1988). Describing the uncertainties in experimental results, *Exp. Therm.*
543 *Fluid Sci.*, **1 (1)**: 3–17.

544 Nema, G., Garimella, S. and Fronk, B. M. (2014). Flow regime transitions during con-
545 densation in microchannels, *Int. J. Refrig.*, **40**: 227–240.

546 Petukhov, B. (1970). Heat transfer and friction in turbulent pipe flow with variable
547 physical properties, *Adv. Heat Transfer*, **6**: 503–564.

548 Qu, W. and Mudawar, I. (2003). Flow boiling heat transfer in two-phase micro-channel
549 heat sinks - I. Experimental investigation and assessment of correlation methods, *Int.*
550 *J. Heat Mass Trans.*, **46 (15)**: 2755–2771.

551 Shah, M. M. (1979). A general correlation for heat transfer during film condensation
552 inside pipes, *Int. J. Heat Mass Tran.*, **22 (4)**: 547–556.

553 Shah, M. M. (2013). General correlation for heat transfer during condensation in plain
554 tubes: further development and verification, *ASHRAE Transactions*, **119**: 3.

555 Shah, M. M. (2016). A condensation for heat transfer during condensation in horizontal
556 mini/micro channels, *Int. J. Refrig.*, **64**: 187–202.

557 Wang, H. and Rose, J. (2005a). Film condensation in horizontal microchannels: effect of
558 channel shape, in *ASME 3rd Int. Conf. Microch. Minich.*, pp. 729–735, American Soc.
559 Mech. Eng.

560 Wang, H. and Rose, J. (2005b). A theory of film condensation in horizontal noncircular
561 section microchannels, *J. Heat Tran.*, **127 (10)**: 1096–1105.

562 Webb, R. and Ermis, K. (2001). Effect of hydraulic diameter on condensation of R-134a
563 in flat, extruded aluminum tubes, *J. Enhanc. Heat Tran.*, **8 (2)**: 77–90.

564 Wu, J., Chen, Y., Shi, M., Fu, P. and Peterson, G. (2009). Three-dimensional numerical
565 simulation for annular condensation in rectangular microchannels, *Nanoscale Micro.*
566 *Thermoph. Eng.*, **13 (1)**: 13–29.

567 Yang, C.-Y. and Webb, R. (1996a). Condensation of R-12 in small hydraulic diameter
568 extruded aluminum tubes with and without micro-fins, *Int. J. Heat Mass Tran.*, **39 (4)**:
569 791–800.

570 Yang, C.-Y. and Webb, R. (1996b). Friction pressure drop of R-12 in small hydraulic
571 diameter extruded aluminum tubes with and without micro-fins, *Int. J. Heat Mass*
572 *Tran.*, **39 (4)**: 801–809.

573 Yang, C.-Y. and Webb, R. (1997). A predictive model for condensation in small hydraulic
574 diameter tubes having axial micro-fins, *J. Heat Tran.*, **119 (4)**: 776–782.

575 Zhang, M. and Webb, R. (2001). Correlation of two-phase friction for refrigerants in
576 small-diameter tubes, *Exp. Therm. Fluid Sci.*, **25 (3-4)**: 131–139.